ROYAL SOCIETY OF CHEMISTRY

PAPER

Check for updates

Effect of Zn–Fe$_2$O$_3$ nanomaterials on the phase separated morphologies of polyvinylidene fluoride piezoelectric nanogenerators

Swathi Yempally,[a] Patricia Magadia[b] and Deepalekshmi Ponnamma [ID] *[c]

Self-powered devices based on piezoelectric nanogenerators (PENGs) are becoming crucial in the upcoming smart societies as they can integrate multifunctional applications, especially sensing, energy storage, *etc.* In this work, we explore the piezoelectric voltage generation happening in polyvinylidene fluoride (PVDF) nanocomposites developed by phase separation. The simple method adopted for the nanocomposite synthesis rules out the high voltage required for the normal electrospun PENGs and adds to their cost-effectiveness. Zinc-doped iron oxide (Zn–Fe$_2$O$_3$) nanomaterials influence the piezoelectric properties by enhancing the crystallinity and structural properties of the polymer. The phase separation process causes structural rearrangements within the PVDF by inducing the directional alignment of −CH$_2$− and −CF$_2$-chains and is the major reason for electroactive phase enhancement. Layers of Zn–Fe$_2$O$_3$ were uniformly distributed in the phase-separated PVDF without being negatively influenced by the solvent-non-solvent interactions during phase separation. At 3 wt%, the Zn–Fe$_2$O$_3$ induced an open circuit voltage of 0.41 volts, about 12 times greater than that of the neat PVDF film. Nanoparticles affected the thermal degradation and crystallinity of the polymer composites most effectively, and the dielectric properties of the PVDF/Zn–Fe$_2$O$_3$ composite microfilms were also pronounced. The proposed simple and cost-effective approach to flexible microfilm fabrication suggests significant applications in wearable electronics.

1. Introduction

Triboelectric and piezoelectric energy harvesting methods offer renewable and promising ways to turn lost mechanical energy into electricity through smarter, flexible, biocompatible, wearable, and eco-friendly platforms.[1–4] Ultra-thin self-powering devices have high demands in wearable electronics and for generating electrical voltage from human body movements. In this regard, flexible piezoelectric polymer nanocomposites of polyvinylidene fluoride (PVDF) and its copolymers have great significance due to their light weight, high processability, and durability as additional benefits.[2,3] Piezoelectric materials convert mechanical energy into electrical energy through electroactive phase variations involving dipole alignments. This happens when a crystalline material like ceramics or polymers with non-central symmetry is mechanically deformed by external forces.[5–7] Lead-free piezoelectric nanomaterials of barium titanate (BaTiO$_3$) and zinc oxide (ZnO), along with

PVDF-based polymeric products, have been extensively investigated in recent years and demonstrated numerous advantages, such as good piezoelectricity, simplicity in structure, ease of synthesis, low production cost, and multifunctional applications.[8] Tuning the band gap of ZnO nanomaterials and their morphologies was extensively studied to test its significance in piezoelectric voltage generation by many research groups, including ours.[9–12] These inorganic ceramic particles always possess several advantages over single crystals, including the ability to transform into various shapes and sizes without being bound by crystallographic orientation.

On the other hand, piezoelectric polymers, like PVDF and its copolymers, have greater piezoelectric stress constants,[13,14] a crucial characteristic of the direct piezoelectric effect when compared to ceramics. Furthermore, their flexibility makes piezoelectric polymeric sensors and actuators easily commercialized through extensive manufacturing and moulded into various shapes. In addition, polymers offer great strength, high impact resistance, low elastic stiffness, high processability, and low density, resulting in a high voltage sensitivity that is ideal for medical and underwater applications, along with low acoustic and mechanical resistance.[14] Hence, hybrid composites of ceramics and polymers with notable piezoelectric properties expect reasonably strong piezoelectricity and flexible deformation features in response to external mechanical energy

[a]Center for Advanced Materials, Qatar University, P.O. Box 2713, Doha, Qatar
[b]Chemical Engineering Department, College of Engineering, Qatar University, 2713, Doha, Qatar
[c]Materials Science and Technology Program, Department of Mathematics, Statistics and Physics, College of Arts and Sciences, Qatar University, 2713, Doha, Qatar. E-mail: deepalekshmi@qu.edu.qa; Tel: +974-50182442

changes. Such nanocomposites are generally developed through specific techniques of poling or electrospinning to align the dipoles within, which is a major prerequisite for exploiting the piezoelectric properties.[15] These expensive methodologies often enhance the challenge of piezoelectric material fabrication, as complete energy utilization cannot be targeted at high voltage expenses. Phase separation is an emerging structural modification method for enriching the electroactive phases in PVDF-based polymers, making dipole alignment feasible for piezoelectricity. Quick and low-cost phase separation processes involving liquid or vapour solvent-non-solvent molecule interactions[16] on the polymer chains report outstanding crystallinity enhancement and piezoelectric sensitivity.[17]

Iron(III) oxide (Fe_2O_3) is a well-known semiconductor material with interesting properties. The doping of Fe_2O_3 into the Zn lattice can create defects and alter the materials' electronic structure, making it more responsive to mechanical stress. By incorporating $Zn–Fe_2O_3$ nanoparticles into PVDF, its piezoelectric performance can be improved, making it useful for sensors and energy harvesting devices. Sahoo *et al.*, recently reported Fe-doped ZnO/PVDF–TrFE composite films fabricated *via* solvent casting with enhanced dielectric, ferroelectric and piezoelectric properties.[18] The idea of nanomaterials doping to enhance the piezoelectric performance of PVDF nanocomposites is extensively studied owing to increased surface charge separation.[19–22] Here, we report a simple and fast nonsolvent-induced phase separation (NIPS) process to develop PVDF-based polymer composites containing $Zn–Fe_2O_3$ nanomaterials. The hybrid nanomaterial $Zn–Fe_2O_3$ was synthesized by the hydrothermal reaction to modify the nanomaterials structurally. The structural modification done on $Zn–Fe_2O_3$ helps to create stronger interactions with the PVDF electroactive phases and provides specific dipole alignments. The phase separation happens when the solvent of polymer dissolution interacts with the non-solvent in the coagulation bath. The selection of a completely miscible solvent–nonsolvent system, the concentration of the polymer solution, the composition of the coagulation bath, and specific conditions for casting the film contribute to the structural and morphological properties of the developed membranes. We could develop piezoelectric properties in the membranes as the phase separation process induces dipole alignment without electrical treatments such as poling. Thus, the present research suggests a low-cost and simple methodology for fabricating piezoelectric nanogenerators based on PVDF nanocomposites.

2. Experimental techniques

2.1. Materials

Polyvinylidene fluoride (PVDF) pellets of molecular weight $M_w = 180 000$ and the solvent N,N-dimethylformamide (DMF) were purchased from Sigma Aldrich. The reactant used to prepare the nanoparticles, iron(III) chloride hexahydrate ($FeCl_3 \cdot 6H_2O$), was purchased from Breckland Scientific Supplies in the UK, zinc acetate dihydrate ($Zn(CH_3CO_2)_2 \cdot 2H_2O$) with a molecular weight $M_w = 219.50$ g mol^{-1} from Bean Town Chemical, USA,

monoethanolamine (MEA) with $M_w = 61.08$ g mol^{-1}, polyethylene glycol (PEG), and ethanol from Sigma Aldrich, Middle East. All chemicals are used without further purification.

2.2. Synthesis of Zn-doped iron oxide

2.622 g $FeCl_3 \cdot 6H_2O$ and 0.073 g $Zn(CH_3CO_2)_2 \cdot 2H_2O$ were dissolved in 50 ml distilled water, to which 0.5 g PEG was added, followed by 3 ml MEA. The resulting solution was transferred into an autoclave, preheated to 120 °C temperature, and then kept for 2 h at the same temperature. After the chemical reaction, the autoclave was allowed to cool. Later the obtained precipitate was washed with ethanol and water several times to remove the soluble ions and dried at 80 °C for 3 h, followed by a 2 h calcination in the tube furnace at 400 °C. The obtained $Zn–Fe_2O_3$ was used for the analysis and composite preparation.

2.3. Phase separation process for PVDF/Zn–Fe$_2$O$_3$ nanocomposite

PVDF pellets (1 g) were dissolved in 10 ml DMF by magnetic stirring for 3 h at 70 °C to obtain a polymer solution. The nanoparticles of $Zn–Fe_2O_3$ were sonicated for 60 min in the same solvent mixture at different weight percentages (1 wt%, 2 wt%, 3 wt%) and were added to the prepared PVDF solution and magnetically stirred overnight. The homogeneous PVDF/$Zn–Fe_2O_3$ composite solution mixture was poured into a Petri dish of diameter 8.5 cm and dried in the oven at 60 °C in a vacuum oven for 4 h. Those casted films were immersed in a coagulation bath containing DMF and water in a 6 : 4 ratio for 3 h for phase separation. The polymer composite films of thickness 130 μm were then removed and thoroughly dried in the vacuum at 40 °C for 30 min. The overall process of phase separation is represented schematically in Fig. 1.

2.4. Characterization techniques

Surface morphology of the nanoparticles as well as composites was analyzed using transmission electron microscope (TEM, FEI TECNAI G2) and scanning electron microscope (SEM, XL-30E Philips Co., Holland). Structural properties of the nano
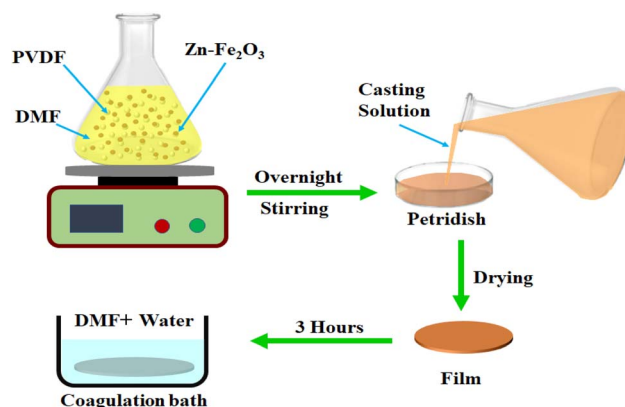

Fig. 1 Schematic representation of the phase separation process of PVDF/Zn–Fe$_2$O$_3$ polymer nanocomposite.
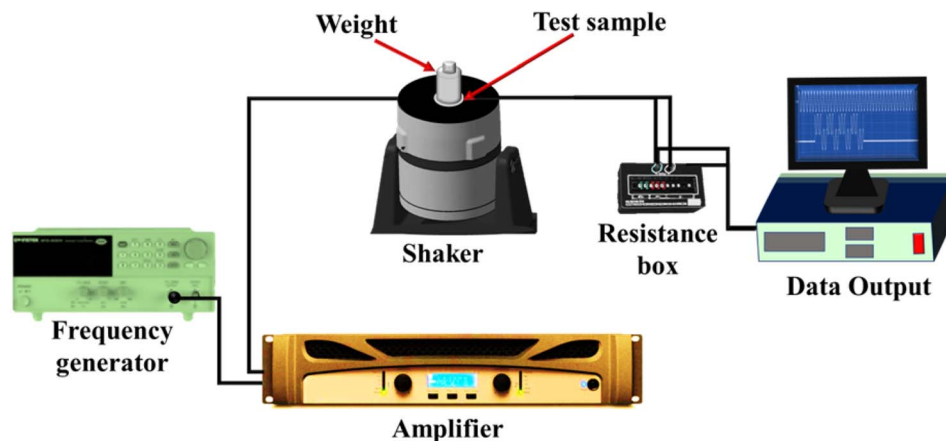
Fig. 2　Schematic illustration of the piezoelectric setup.

powder and the polymer membranes were studied using an XRD diffractometer (EMPYREAN, PANalytical Co., Almelo, Netherlands) within the 2θ range of 10° to 80°, using the CuKα radiation ($\lambda = 0.1564$ nm) operated at 45 kV/40 mA. A Fourier transformation infrared spectrometer (FTIR, PerkinElmer Spectrum 400) in transmission mode was used to study the phase variation of polymer composites in a range of 500–4000 cm^{-1} with a resolution of 2 cm^{-1}. The atomic force microscopy analysis was carried out to study the surface topography and surface roughness using the microscope MFP-3D, Asylum Research, USA. Dielectric frequency sweep measurements were done by a broad-band dielectric/impedance spectroscope (Novocontrol) in the frequency range 10^{-2} to 10^{7} Hz. The crystallinity of the samples was determined using a PerkinElmer DSC4000 differential scanning calorimeter. The samples were treated between 20 °C and 200 °C at 10 °C min^{-1} under a nitrogen atmosphere for a complete heating–cooling–heating cycle. The thermal stability analysis of samples was done by the thermogravimetric analyzer (TGA), the PerkinElmer TGA 4000, at a heating rate of 10 °C min^{-1} from 30–600 °C under a nitrogen atmosphere. The piezoelectric output voltage properties of the samples were tested using an assembled lab setup consisting of an amplifier, frequency generator, VTS vibration system, cylindrical mass with a force of 2.5 N to keep on the sample, and a resistance box connected to an NI (National Instrument) instrument as shown in Fig. 2.[11]

3.　Results and discussion

3.1.　Morphology and structural investigation of Zn–Fe$_2$O$_3$ nanoparticles

The morphology of the Zn–Fe$_2$O$_3$ nanomaterials was tested using the TEM images. Fig. 3a and b show the TEM images of Zn–Fe$_2$O$_3$ at 50 nm and 100 nm resolutions. Fig. 3a shows plate-like Zn–Fe$_2$O$_3$ structures with the width of the layers ranging from 25–30 nm. As shown in Fig. 3b, distinctive plate-like features of Fe$_2$O$_3$ nanoparticles are prominent throughout at lower magnification. XRD pattern of the as-prepared Zn–Fe$_2$O$_3$

nanomaterials is shown in Fig. 3c. The obtained diffractogram peaks at 2θ values, 24.1°, 33.2°, 41.0°, 49.5° and 64.1°, respectively, correspond to (012), (110), (113), (024) and (300) crystal planes. This indicates the presence of a rhombohedral Fe$_2$O$_3$ structure for the composite powder. XRD spectra also contain characteristic peaks at 2θ values 55.4°, 62.3° corresponding to the (003), (103) planes of composite.[23] A slight deviation of the peaks from the reported XRD pattern for Fe$_2$O$_3$ indicates the successful incorporation of Zn in the Fe$_2$O$_3$ structure. The sharp diffraction peak pattern further confirms the ultra-high crystallinity of the synthesized nanoparticles.[24]

FTIR spectroscopy is utilized to detect the presence of functional groups on the surface of the synthesized Zn–Fe$_2$O$_3$. In the FTIR spectrum, the Fe–O bond vibrations of Fe$_2$O$_3$ were observed at wavenumber 551.8 cm^{-1} and 608.1 cm^{-1}. Moreover, a broadband corresponding to the surface hydroxide functional groups was observed at 3376 cm^{-1}. These stretching vibrations of FTIR spectra indicate the presence of α-Fe$_2$O$_3$. The peak at 1648 cm^{-1} is assigned to C=O stretching vibrations shown in Fig. 3d.[24]

3.2.　Morphology and structural investigation of PVDF/Zn–Fe$_2$O$_3$ polymer nanocomposite

The surface morphology of the neat PVDF and the PVDF composites with the incorporation of Zn–Fe$_2$O$_3$ nanofillers is investigated by SEM analysis. As shown in Fig. 4a, the neat PVDF shows a spherulite morphology of average 9.0 μm size, indicating the presence of PVDF α-phase. After adding Zn–Fe$_2$O$_3$ nanofillers in different weight percentages, the size of the spherulites substantially reduced. For the 3% Zn–Fe$_2$O$_3$ the size of spherulites reached to about 4.0 μm. The crystallization kinetics of the polymer are reflected in the size of the spherulite. It is based on both the fillers' capacity for nucleation and the growth rate of the spherulites. It is well known that adding nanofillers provides more nucleation sites, producing smaller spherulite structures than the neat PVDF, as shown in Fig. 4b–d. Jaleh *et al.* reported similar observations with respective changes in the spherulite size.[25] In most cases, the interaction of nanoparticles with PVDF chains causes the phase change of
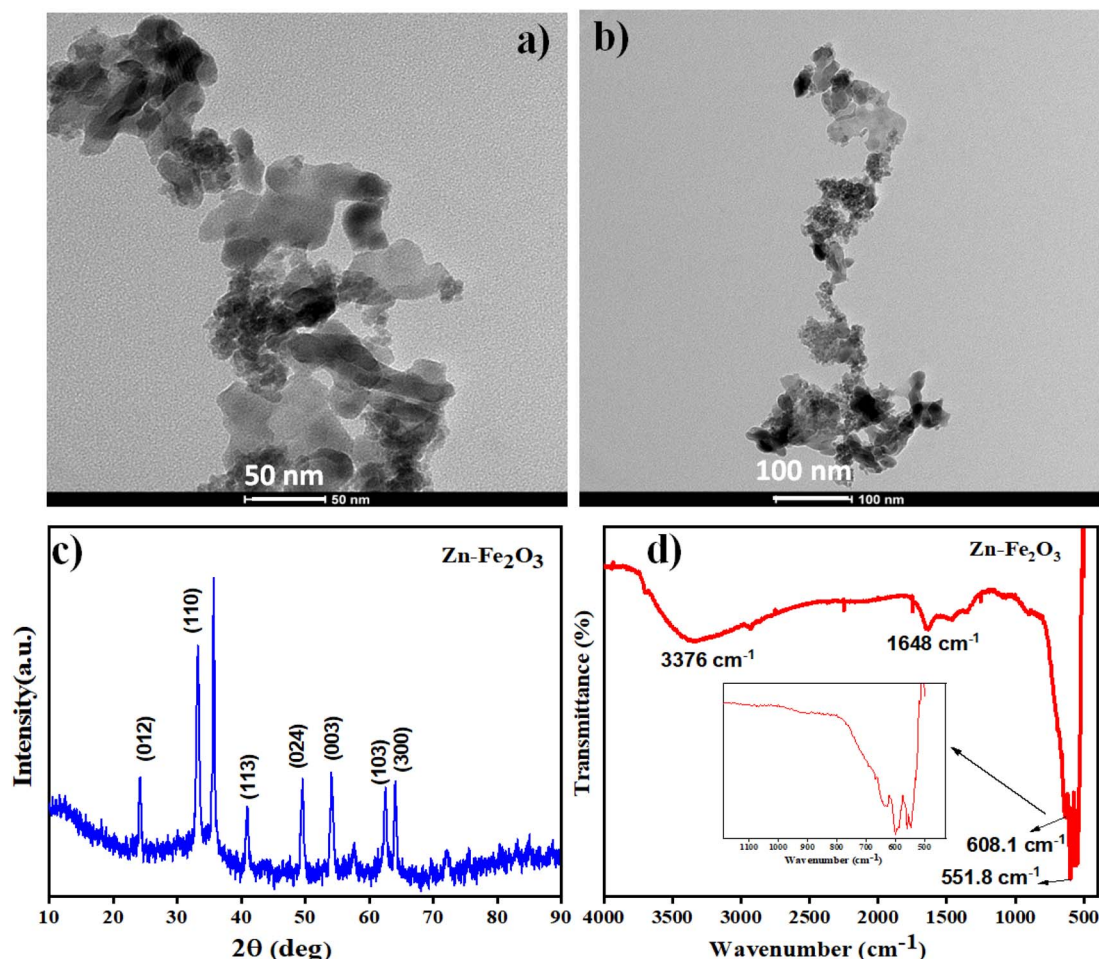
Fig. 3 (a) and (b) TEM images and (c) and (d) XRD and FTIR pattern of Zn–Fe$_2$O$_3$ nanoparticle.

PVDF (α-phase to β-phase as indicated by XRD and FTIR). During the crystal growth, these interactions in PVDF segments further propagate to induce enhanced nucleation. Hence, there must be some connection between the induction of morphological changes and crystal nucleation in PVDF crystallization.[26]

EDX mapping was done to confirm the elemental distribution in the synthesized composites. The representative EDX images of 1%, 2% and 3% of PVDF/Zn–Fe$_2$O$_3$ polymer nanocomposite are shown in Fig. 5. It is demonstrated in Fig. 5 that with the increase in nanofillers weight percentage, the PVDF structure's spherical size decreases gradually. The EDX image of 1% PVDF/Zn–Fe$_2$O$_3$ composite confirms the presence of metals, Zn and Fe uniformly distributed in the PVDF matrix as shown in Fig. 5a. There were no other trace elements/impurities observed in any of the EDX images, confirming the high purity of as-synthesized polymer composites. Similarly, the 2% and 3% PVDF/Zn–Fe$_2$O$_3$ EDX images also exhibit the distribution of relevant elements as expected.

The crystallinity and morphology of PVDF/Zn–Fe$_2$O$_3$ polymer composites were investigated using XRD and SEM analysis. The XRD pattern of the polymer nanocomposite, as shown in Fig. 6a, shows a unique peak at 2θ value 20.3° corresponding to the

planes (110) and (200) of polar phase PVDF (β + γ-phase) in all the polymer composites of various compositions. Gregorio *et al.*, attributed the peak at 2θ value 20.26° to the piezoelectric active β-phase.[27] At a lower percentage of 1% PVDF/Zn–Fe$_2$O$_3$, the α-PVDF phase is also observed 2θ value of 19.8° corresponds to the plane (110).[28] Whereas γ-phase PVDF is predominately observed 2θ value 40.2° corresponds at the plane (211) at higher concentrations of 3% PVDF/Zn–Fe$_2$O$_3$. From the XRD pattern, it is concluded that the inclusion of nanofiller Zn–Fe$_2$O$_3$ facilitated the exclusive formation of γ-phase PVDF suitable for the piezoelectric application. The pure PVDF XRD pattern exhibits peak patterns characteristics of both α and γ-PVDF crystalline phases. The FTIR spectrum representing the characteristic stretching vibrations of pure PVDF film and the polymeric PVDF composites with different weight percentages of nanofillers is shown in Fig. 6b. The major peaks corresponding to γ-PVDF at 1234 cm^{-1} and 834 cm^{-1} are observed in all the compositions. A negligible peak shift in the FTIR spectrum is observed with an increase in the weight percentage of the nanofiller PVDF film. FTIR data are often utilized to estimate the polar phase percentages of the PVDF composite film. Lambert Beer law was used to obtain the absorption coefficients, $A(\alpha)$ and $A(\beta)$ at wavenumbers 766 cm^{-1} and 840 cm^{-1}. According to Gregorio
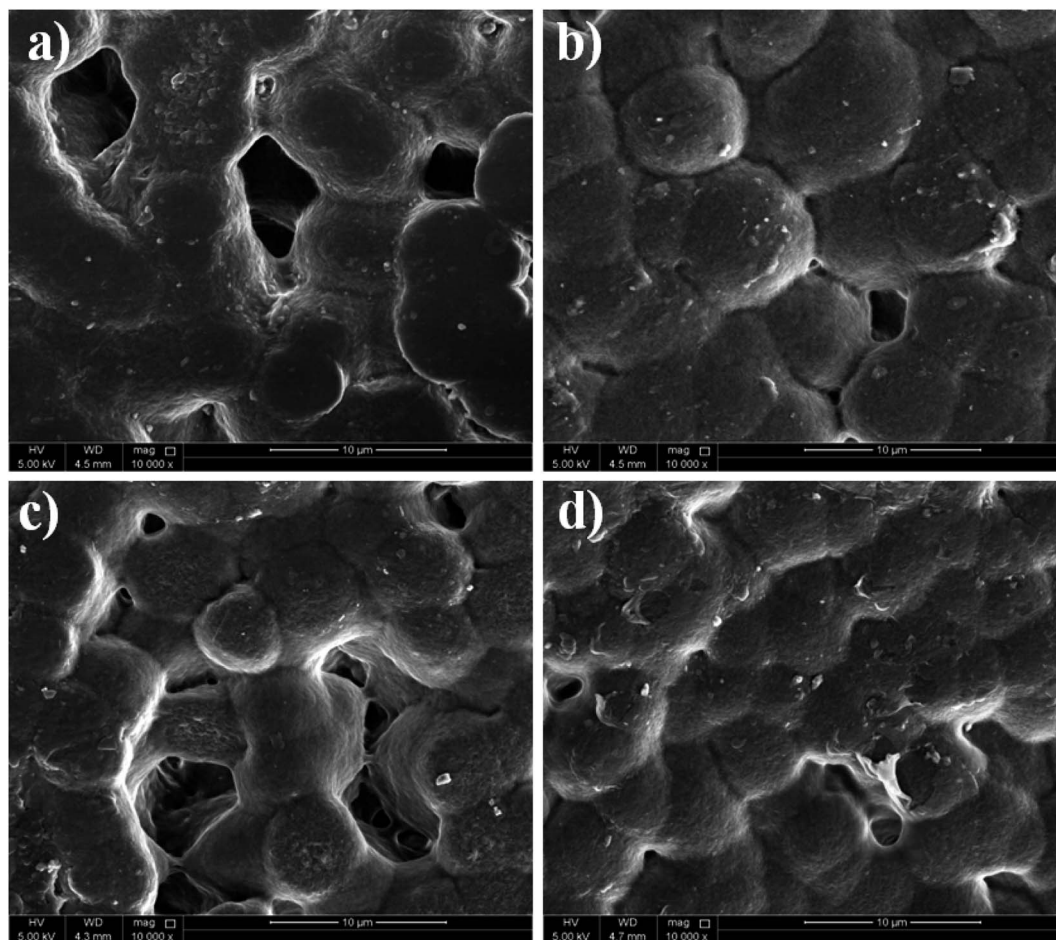
Fig. 4 Scanning electron microscope (SEM) images of (a) neat PVDF, (b) 1%, (c) 2% and (d) 3% of PVDF/Zn–Fe$_2$O$_3$ polymer nanocomposite.
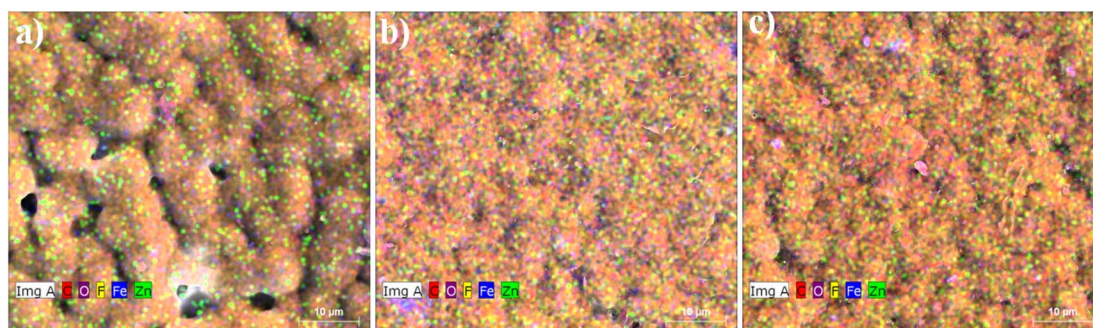

Fig. 5 The energy dispersive spectroscopy (EDX) images of (a) 1%, (b) 2% and (c) 3% of PVDF/Zn–Fe$_2$O$_3$ polymer nanocomposite.

et al. the relative fraction of the β-phase in a sample containing PVDF is as follows:[29]

$$F(\beta) = \frac{X_\beta}{X_\alpha + X_\beta} = \frac{A_\beta}{1.26A_\alpha + A_\beta} \qquad (1)$$

where X_α and X_β are the crystalline mass fractions of the α and β phases. The polar phase percentages of the pure PVDF and PVDF with Zn–Fe$_2$O$_3$ filler with weight percentages are given in Table 1.

Surface morphology of PVDF/Zn–Fe$_2$O$_3$ nanocomposite thin films was further analyzed by atomic force microscopy (AFM), illustrating the three-dimensional topographic images acquired through tapping mode of (a) neat PVDF, (b) 1% PVDF/Zn–Fe$_2$O$_3$, (c) 2% PVDF/Zn–Fe$_2$O$_3$, (d) 3% PVDF/Zn–Fe$_2$O$_3$ are shown in Fig. 7a–d. It is clear from the image that the neat PVDF has a smoother surface than the composites made of other PVDF/ Zn–Fe$_2$O$_3$. The quantitative studies results show that average surface roughness (R_a) is increasing from 4.24 nm to 10.41 nm
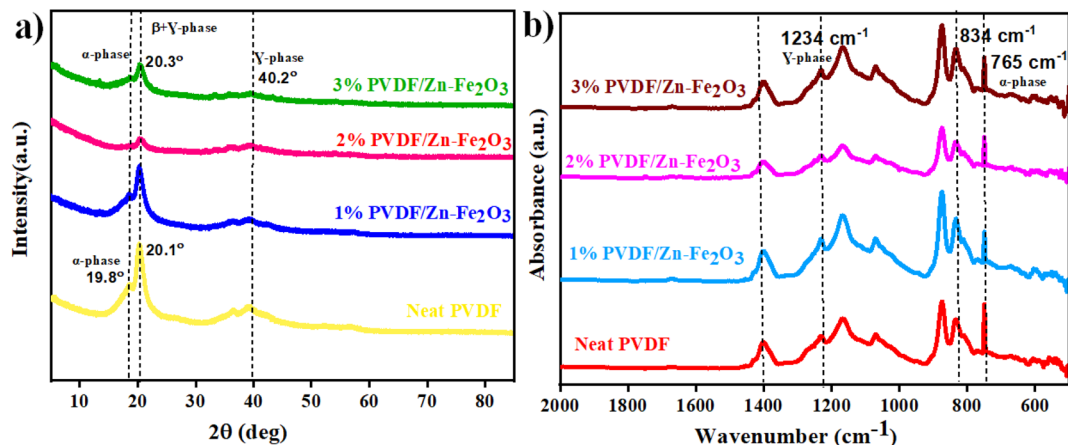
Fig. 6 (a) XRD and (b) FTIR patterns of the PVDF/Zn–Fe$_2$O$_3$ composite with different filler contents.

Table 1 Refractive fraction of calculated polar phase content

Sample name	$F(\beta)$ (%)
Neat PVDF	34.20
1% PVDE/Zn–Fe$_2$O$_3$	39.27
2% PVDE/Zn–Fe$_2$O$_3$	40.25
3% PVDF/Zn–Fe$_2$O$_3$	41.48

leading to a two-times increase in the surface roughness with increasing in the percentage of filler composites of Zn–Fe$_2$O$_3$ which is mostly due to the increase in the homogeneous distribution of fillers on the PVDF surface. Also, a similar trend can be seen for root mean square surface roughness ($R_{\rm m}$) from 5.84 nm to 13.40 nm for the neat PVDF to 3% PVDF/Zn–Fe$_2$O$_3$. Previous studies confirm that adding nanoparticles to the PVDF/Zn–Fe$_2$O$_3$ matrix causes an increase in surface roughness.[30,31] This is attributed to the nature and dispersion of fillers, morphology, and the polymer–filler interactions. Fillers create localized areas within the composites, which influence the composite properties according to the functionality.

3.3. Thermal stability of PVDF/Zn–Fe$_2$O$_3$ polymer nanocomposite

The thermogravimetric and derivative thermogravimetric curves were obtained for the PVDF composite, as shown in Fig. 8a. The thermal stability of the PVDF composite is enhanced with the addition of Zn–Fe$_2$O$_3$ nanofillers. The neat PVDF starts degrading at 420 °C, whereas the PVDF composite with 3% PVDF/Zn–Fe$_2$O$_3$ decomposes at 466 °C. This enhancement in thermal stability can be attributed to the high distribution of inorganic nanofillers within the polymer matrix, thereby minimizing the moment of PVDF chains by nanofillers.[32] All the polymer nanocomposites show similar decomposition pathways, as shown in Fig. 8a. The initial weight loss at 447.0 °C is due to the rupture in the polymeric chains of PVDF. The second weight loss at 483.2 °C can be assigned to the complete decomposition of the polymeric composite. The DTA curves for all the composites with varying concentrations of Zn–

Fe$_2$O$_3$ are shown in Fig. 8b. The decomposition temperatures from the DTA curves for 1% PVDF/Zn–Fe$_2$O$_3$, 2% PVDF/Zn–Fe$_2$O$_3$ and 3% PVDF/Zn–Fe$_2$O$_3$ are 467.4 °C, 477.2 °C and 478.9 °C respectively.

The polymer composites show higher weight loss values when compared to the neat polymer, and this behaviour can be because of the high thermal conductivity of the filers and their uniform distribution in the polymer medium.

3.4. Melting and crystallization behaviour of PVDF/Zn–Fe$_2$O$_3$ polymer composite

The melting and crystallization behaviours measurements for PVDF and PVDF/Zn–Fe$_2$O$_3$ polymer composite are performed by a DSC analyzer to understand the effect of nanofillers on the melting temperature and degree crystallinity of the synthesized PVDF nanocomposites. The DSC analysis curve indicates the crystallization temperature ($T_{\rm c}$) of about 128.1 °C for the neat PVDF, which is shifted to 130.4 °C with the addition of 1% PVDF/Zn–Fe$_2$O$_3$. It is observed that with further increase in the weight percentage of Zn–Fe$_2$O$_3$, the $T_{\rm c}$ value also increases linearly to the higher temperatures of 2% PVDF/Zn–Fe$_2$O$_3$ and 3% PVDF/Zn–Fe$_2$O$_3$ with crystalline temperatures 131.3 °C and 132.6 °C respectively as shown in Fig. 9b. The illustrate report suggest that the γ-phase possess higher $T_{\rm c}$ compares to the α-phase.[33,34] As a result, the shift in $T_{\rm c}$ to higher temperatures supports the transformation from α-phase PVDF to γ-phase PVDF, consistent with the FTIR results. The melting temperature ($T_{\rm m}$) of neat PVDF occurs at 158.2 °C whereas the $T_{\rm m}$ values for 1% PVDF/Zn–Fe$_2$O$_3$, 2% PVDF/Zn–Fe$_2$O$_3$ and 3% PVDF/Zn–Fe$_2$O$_3$ were observed at 160.5 °C, 159.4 °C and 159.8 °C respectively as shown in Fig. 9a. This shift in ($T_{\rm m}$) to higher temperatures in polymeric composites is indicative of PVDF transition into a different phase than neat PVDF. The melting and crystallization temperatures of composites containing filler particles are higher than those of the neat PVDF (Fig. 9a and b). This is owing to the presence of nanofillers that act as nucleating agents.[11,35] The addition of Zn–Fe$_2$O$_3$ nanoparticles appears to have resulted in larger crystallite sizes, which resulted in a higher melting temperature. The DSC results show

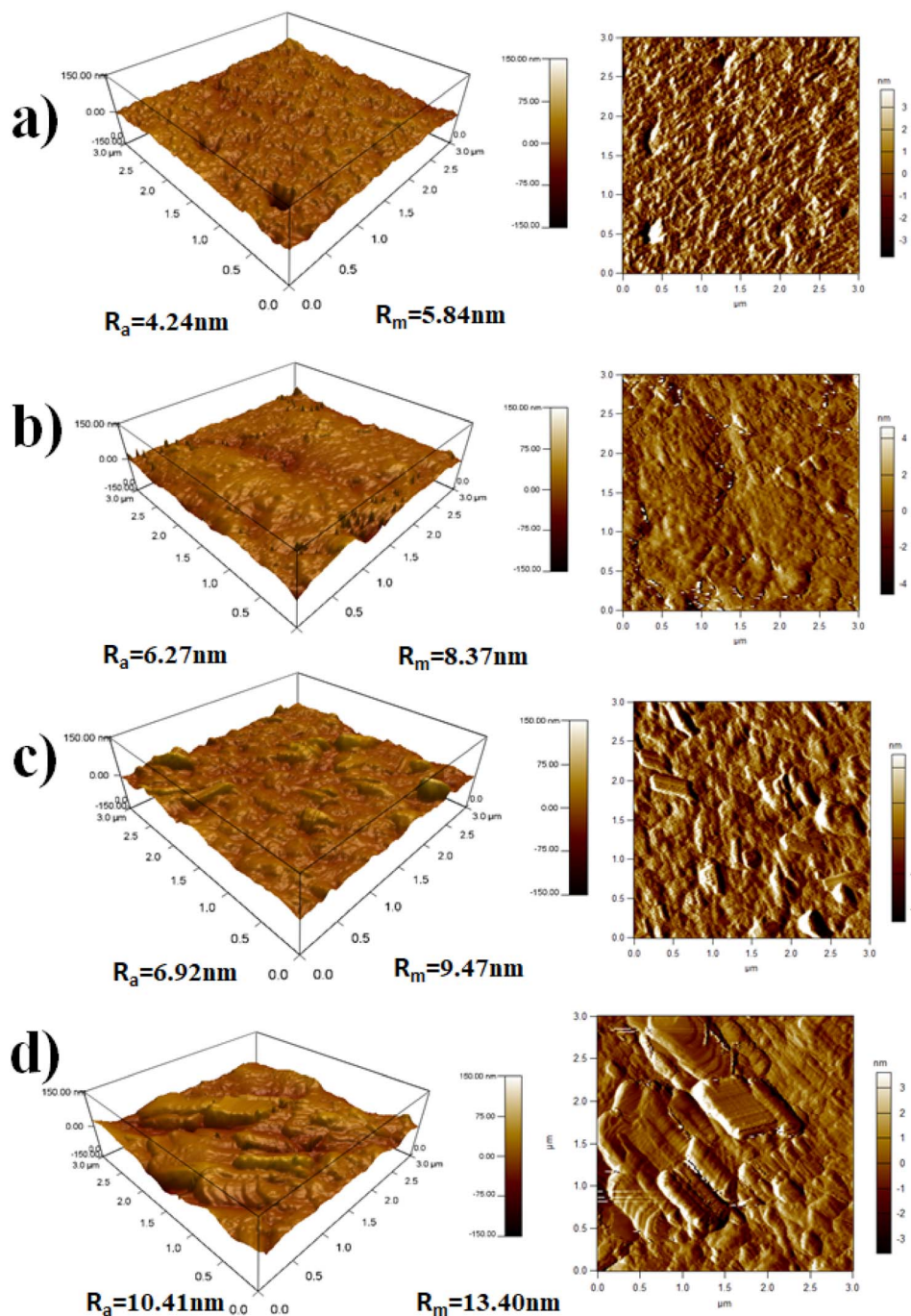© 2023 The Author(s). Published by the Royal Society of Chemistry

Fig. 7 The AFM micrograph with the 3D topographic profile of the surface roughness of (a) neat PVDF, (b) 1%, (c) 2% and (d) 3%, of PVDF/Zn–Fe$_2$O$_3$ polymer nanocomposite.

that the Zn–Fe$_2$O$_3$ composites have improved γ-phase, which agrees with the XRD and FTIR data.

3.5. Dielectric properties of PVDF/Zn–Fe$_2$O$_3$ polymer composites

Broadband dielectric spectroscopy is an effective method for exploring the molecular dynamics of polymer composites because significant information about these processes may be obtained over a broad frequency (milli to mega) hertz at room temperature range.[36] The frequency-dependent dielectric constant and loss values for neat PVDF and its PVDF/Zn–Fe$_2$O$_3$ composites of different weight percentages are represented in Fig. 10a and b, respectively. According to Fig. 10a, the dielectric constant increases by adding different weight percentages of Zn–Fe$_2$O$_3$ filler, reaching its highest value (approximately three times greater than the neat PVDF polymer). Due to the free charge carrier movement caused by the continuous conductive networks of filler particles, the dielectric constant and loss
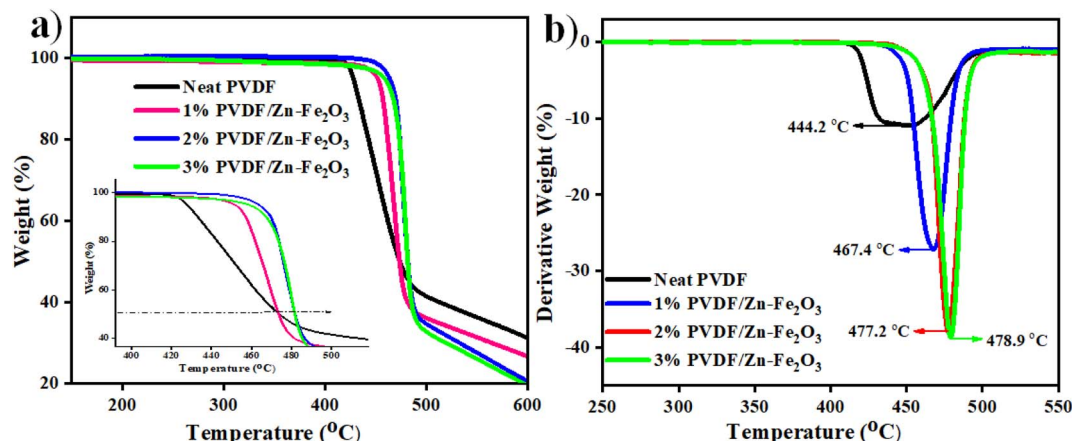
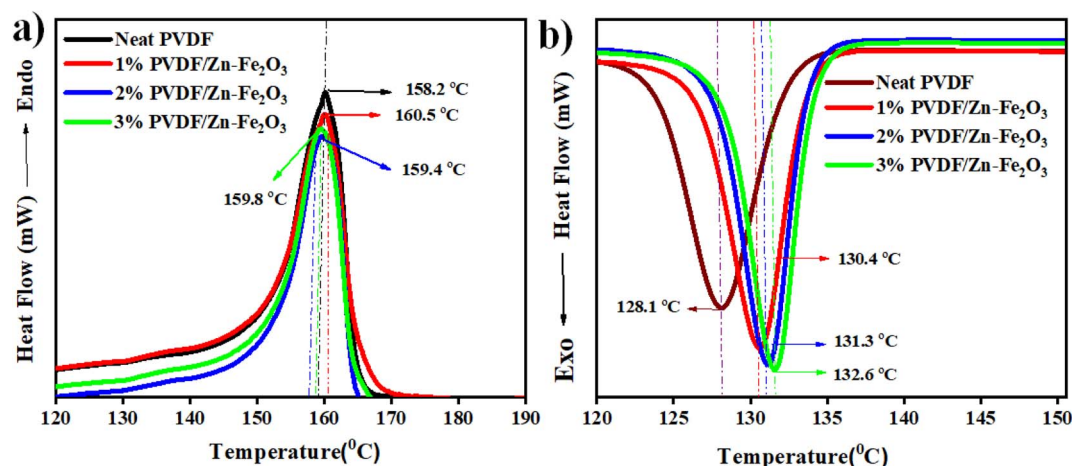**Fig. 8**   (a) TGA (b) DTA curves of PVDF/Zn–Fe$_2$O$_3$ polymer nanocomposite.

Fig. 9   DSC curves of neat PVDF and PVDF/Zn–Fe$_2$O$_3$ composites. (a) First cooling scan; (b) second heating scan.

increase follows a similar trend. The enhanced dielectric constant with filler addition can be correlated with the Maxwell–Wagner–Sillars (MWS) interfacial polarization effect.[37] According to this effect, at the polymer–filler interface, space charges accumulate, and short-range dipole–dipole interactions occur, causing interfacial polarization and thus increasing the dielectric constant.[38] The previous studies suggest that with the addition of ZnO nanofillers, charge carriers likely to be trapped on the polymer's upper surface.[39] If these charge carriers cause homocharge layers near the electrodes, space charge production will rise. This explains why the amount of charges in nanocomposites with adequate dispersion of Zn–Fe$_2$O$_3$ nanoparticles is greater than in neat PVDF. When Fe was doped with ZnO, the interaction between the filler and the matrix was different. Because of the conducting nature of Fe charge accumulation at the Zn–Fe$_2$O$_3$ interface happened more effectively under the applied field. As a result of this charge accumulation, space charge polarization increased, which further improved dielectric permittivity.[40,41] However, apart from the MWS effect, the increased electroactive β-phase content in the composite contributes to an increase in the dielectric constant. Due to its

stronger frequency dependence and networking effect, the dielectric constant of the polymer composite decreases sharply with frequency enhancement compared to the neat PVDF polymer.[42,43] The low number of aligned dipoles causes the dielectric constant to decrease.

Because of the presence of Zn–Fe$_2$O$_3$ nanoparticles, the conductivity and tan δ values illustrated in Fig. 10c and d for all the samples were slightly increased with the frequency of the filler-added system. Because of the interfacial polarization effect, the conductivity values gradually increase with the weight percentages of the nanofillers added to neat PVDF with increased frequency.[44] The conductivity values increase with the number of charge carriers in the system, resulting in the uniformly distributed Zn–Fe$_2$O$_3$ at 3 wt% shows the highest value, as shown in Fig. 10.

3.6.   Piezoelectric study of PVDF/Zn–Fe$_2$O$_3$ polymer composite

The PVDF/Zn–Fe$_2$O$_3$ composite films were cut into circular pieces of 2 cm diameter, and silver paste was polished on the
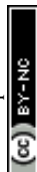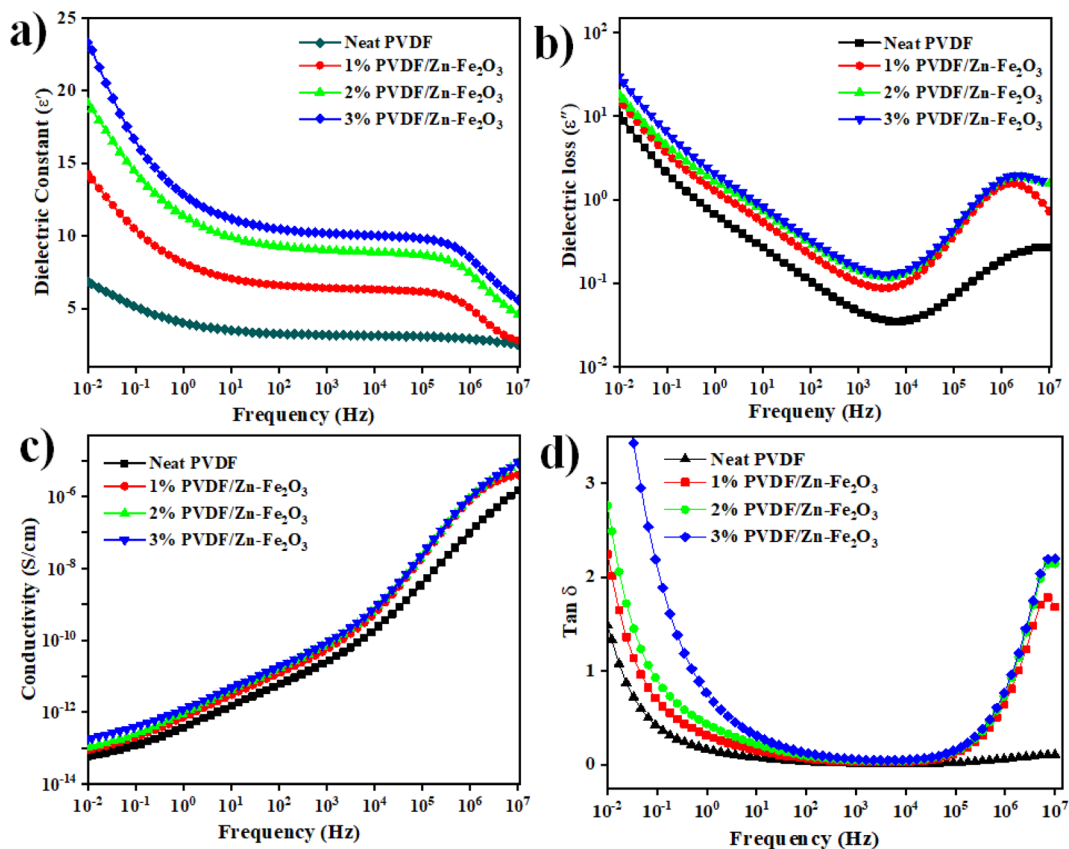
Fig. 10 (a) and (b) Variation of dielectric constant and dielectric loss. (c) and (d) Conductivity and tan of neat PVDF, 1%, 2%, and 3% of PVDF/Zn–Fe$_2$O$_3$ polymer composite with frequency.

top and bottom surfaces of a PVDF film. For output voltage measurement, the setup, as shown in Fig. 2, has been employed as per the established procedure.[11,12] To avoid direct contact between two electrodes, a small gap of approx. 2 mm was created between the silver paste's edge and the PVDF film's edge. Two pieces of copper tape were connected to both ends of
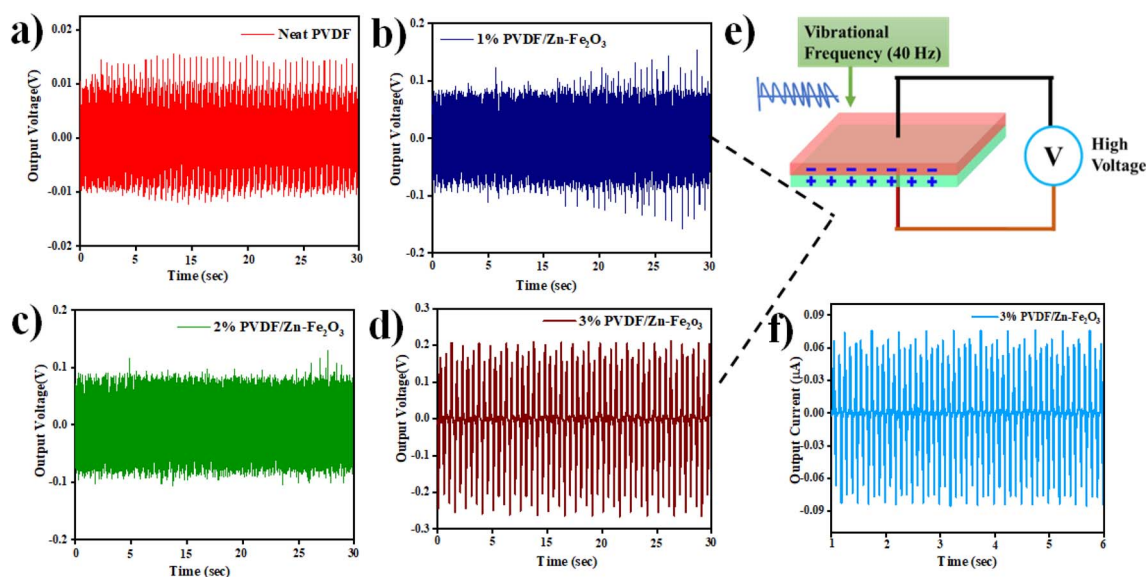

Fig. 11 Piezoelectric output voltage for phase separation process of (a) neat PVDF (b) 1% PVDF/Zn–Fe$_2$O$_3$ (c) 2% PVDF/Zn–Fe$_2$O$_3$ (d) 3% PVDF/Zn–Fe$_2$O$_3$ polymer composite with piezoelectric setup (shown in Fig. 2). (e) Mechanism involved in piezoelectricity and (f) output current for 3% PVDF/Zn–Fe$_2$O$_3$.
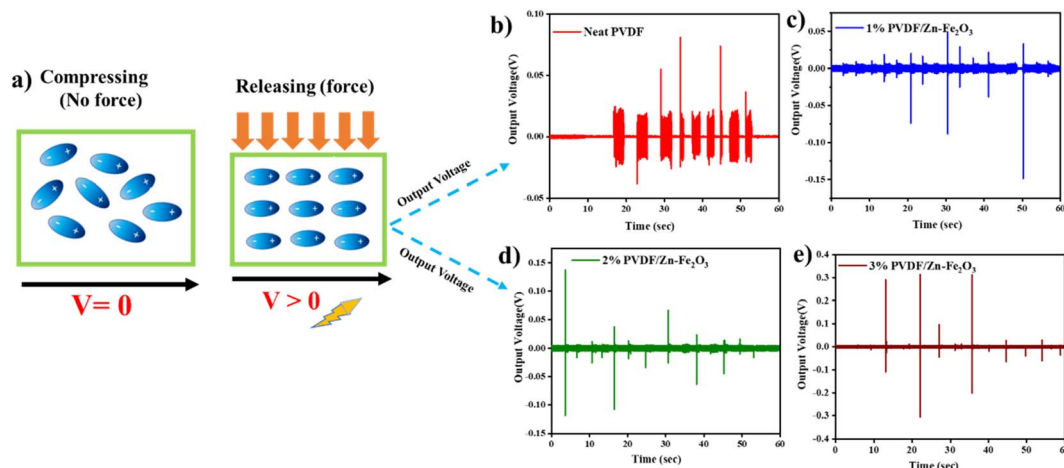
Fig. 12 The piezoelectric output voltage for the phase separation process with working mechanism of compressing and releasing of (a) schematic illustration of the piezoelectric effect (b) neat PVDF (c) 1% PVDF/Zn–Fe$_2$O$_3$ (d) 2% PVDF/Zn–Fe$_2$O$_3$ (e) 3% PVDF/Zn–Fe$_2$O$_3$ polymer composite.

the electrodes for electromechanical measurement. All the composite films (1%, 2%, and 3% of PVDF/Zn–Fe$_2$O$_3$) showed enhanced output voltage compared to the neat PVDF film. This enhanced output performance can be attributed to the increased γ-phase induced by the presence of Zn–Fe$_2$O$_3$ nanofillers. Similar observations of improvements in the output voltage were also observed by Mandal *et al.*[45] The average thickness of all the polymer composite films was measured at ~130 μm thick. The highest peak–peak output voltage of 0.41 V was observed for the film containing 3% PVDF/Zn–Fe$_2$O$_3$ and is ~12 times greater than the neat PVDF film (0.032 V) as shown in Fig. 11. The output short circuit current shown in the Fig. 11f for 3% PVDF/Zn–Fe$_2$O$_3$ is 0.16 μA which is ~26 times higher than the current observed in the case of neat PVDF film. As evidenced by DSC results, the increase in the nanofiller concentration facilitates the formation of electroactive β-phase PVDF film, therefore further assisting the improvement in the output voltage when the nanofillers are used.[46,47]

The peak–peak output voltage was also measured by a simple finger press technique, *i.e.*, compressing and releasing[47] by replacing the shaker to test the real-time application. Piezoelectric signals will be generated in the stages of pressing and releasing. As expected, the 3% PVDF/Zn–Fe$_2$O$_3$ composite output voltage of 0.617 V is 21 times greater than the output voltage observed in the case of neat PVDF film (0.029 V). Moreover, with the increase in the nanofiller concentration, the output voltage also increased, as shown in Fig. 12. A similar trend was observed when the shaker was used to apply pressure.

4. Conclusion

In summary, we successfully synthesized Zn-doped iron oxide nanoparticles by hydrothermal process. The phase separation process developed neat PVDF and its nanocomposites with different concentrations, 1 wt%, 2 wt%, and 3 wt% of Zn–Fe$_2$O$_3$ nanoparticles. The surface morphology of the composites was revealed by SEM and AFM studies based on the concentration of

Zn–Fe$_2$O$_3$ nanoparticles within the polymer. The dielectric studies revealed that increasing the filler concentrations improved the electrical properties of the PVDF/Zn–Fe$_2$O$_3$. The polymer composite developed by phase separation process with the 3 wt% PVDF/Zn–Fe$_2$O$_3$ produced an open circuit voltage of 0.41 V which is ~12 times greater than the neat PVDF polymer film. The investigation on the piezoelectric properties revealed good piezoelectric performance for the 3 wt% PVDF/Zn–Fe$_2$O$_3$.

Conflicts of interest

There are no conflicts to declare.

Acknowledgements

References

1 N. Meng, X. Ren, G. Santagiuliana, L. Ventura, H. Zhang, J. Wu, H. Yan, M. J. Reece and E. Bilotti, Ultrahigh β-phase content poly(vinylidene fluoride) with relaxor-like ferroelectricity for high energy density capacitors, *Nat. Commun.*, 2019, **10**(1), 4535.

2 A. M. AlAhzm, M. O. Alejli, D. Ponnamma, Y. Elgawady and M. A. Al-Maadeed, Piezoelectric properties of zinc oxide/ iron oxide filled polyvinylidene fluoride nanocomposite fibers, *J. Mater. Sci.: Mater. Electron.*, 2021, **32**(11), 14610– 14622.

3 Y. Cho, J. Jeong, M. Choi, G. Baek, S. Park, H. Choi, S. Ahn, S. Cha, T. Kim, D. S. Kang and J. Bae, BaTiO$_3$@PVDF-TrFE nanocomposites with efficient orientation prepared via

phase separation nano-coating method for piezoelectric performance improvement and application to 3D-PENG, *Chem. Eng. J.*, 2022, **427**, 131030.

4 Y. Guo, X. S. Zhang, Y. Wang, W. Gong, Q. Zhang, H. Wang and J. Brugger, All-fiber hybrid piezoelectric-enhanced triboelectric nanogenerator for wearable gesture monitoring, *Nano Energy*, 2018, **48**, 152–160.

5 Q. Zhu, T. Wu and N. Wang, From Piezoelectric Nanogenerator to Non-Invasive Medical Sensor: A Review, *Biosensors*, 2023, **13**(1), 113.

6 V. F. Cardoso, C. M. Costa, D. M. Correia, E. O. Carvalho, N. Peřinka, P. M. Martins, R. M. Meira, T. Marques-Almeida, T. Rodrigues-Marinho and S. Lanceros-Mendez, Solution processing of piezoelectric unconventional structures, in *Organic Ferroelectric Materials and Applications*, Woodhead Publishing, 2022, pp. 375–439.

7 V. E. Ogbonna, A. P. Popoola and O. M. Popoola, Piezoelectric Ceramics Materials on Transducer Technology for Energy Harvesting: A Review, *Frontiers in Energy Research*, 2022, 1917.

8 D. Hu, M. Yao, Y. Fan, C. Ma, M. Fan and M. Liu, Strategies to achieve high performance piezoelectric nanogenerators, *Nano Energy*, 2019, **55**, 288–304.

9 M. Ghosh and M. G. Rao, Growth mechanism of ZnO nanostructures for ultra-high piezoelectric d_{33} coefficient, *Mater. Express*, 2013, **3**(4), 319–327.

10 V. Cauda, S. Stassi, A. Lamberti, M. Morello, C. F. Pirri and G. Canavese, Leveraging ZnO morphologies in piezoelectric composites for mechanical energy harvesting, *Nano Energy*, 2015, **18**, 212–221.

11 H. Parangusan, D. Ponnamma and M. A. AlMaadeed, Flexible tri-layer piezoelectric nanogenerator based on PVDF-HFP/Ni-doped ZnO nanocomposites, *RSC Adv.*, 2017, **7**(79), 50156–50165.

12 H. Parangusan, D. Ponnamma and M. A. Al-Maadeed, Stretchable electrospun PVDF-HFP/Co-ZnO nanofibers as piezoelectric nanogenerators, *Sci. Rep.*, 2018, **8**(1), 754.

13 J. P. Pereira, P. Costa and S. Lanceros-Méndez, Piezoelectric energy production, *Compr. Energy Syst.*, 2018, **3**(5), 380–415.

14 K. K. Sappati and S. Bhadra, Piezoelectric polymer and paper substrates: a review, *Sensors*, 2018, **18**(11), 3605.

15 X. Liu, J. Ma, X. Wu, L. Lin and X. Wang, Polymeric nanofibers with ultrahigh piezoelectricity via self-orientation of nanocrystals, *ACS Nano*, 2017, **11**(2), 1901–1910.

16 X. Wang, D. Chen, T. He, Y. Zhou, L. Tian, Z. Wang and Z. Cui, Preparation of Lateral Flow PVDF Membrane via Combined Vapor-and Non-Solvent-Induced Phase Separation (V-NIPS), *Membranes*, 2023, **13**(1), 91.

17 T. Huang, S. Yang, P. He, J. Sun, S. Zhang, D. Li, Y. Meng, J. Zhou, H. Tang, J. Liang and G. Ding, Phase-separation-induced PVDF/graphene coating on fabrics toward flexible piezoelectric sensors, *ACS Appl. Mater. Interfaces*, 2018, **10**(36), 30732–30740.

18 R. Sahoo, S. Mishra, L. Unnikrishnan, S. Mohanty, S. Mahapatra, S. K. Nayak, S. Anwar and A. Ramadoss, Enhanced dielectric and piezoelectric properties of Fe-doped ZnO/PVDF-TrFE composite films, *Mater. Sci. Semicond. Process.*, 2020, **117**, 105173.

19 M. A. Hari, S. C. Karumuthil, S. Varghese and L. Rajan, Performance enhancement of flexible and self-powered PVDF-ZnO based tactile sensors, *IEEE Sens. J.*, 2022, **22**(10), 9336–9343.

20 M. Kim and J. Fan, Piezoelectric properties of three types of PVDF and ZnO nanofibrous composites, *Adv. Fiber Mater.*, 2021, **3**(3), 160–171.

21 S. Mansouri, T. F. Sheikholeslami and A. Behzadmehr, Investigation on the electrospun PVDF/NP-ZnO nanofibers for application in environmental energy harvesting, *J. Mater. Res. Technol.*, 2019, **8**(2), 1608–1615.

22 W. Deng, T. Yang, L. Jin, C. Yan, H. Huang, X. Chu, Z. Wang, D. Xiong, G. Tian, Y. Gao and H. Zhang, Cowpea-structured PVDF/ZnO nanofibers based flexible self-powered piezoelectric bending motion sensor towards remote control of gestures, *Nano Energy*, 2019, **55**, 516–525.

23 P. Khalili and M. Farahmandjou, Study of α-Fe₂O₃@ZnO nanoleaves: morphological and optical study, *Materials Engineering Research*, 2020, **2**(1), 118–124.

24 Comparative Structural Properties of Nanosized ZnO/Fe₃O₄ Composites Prepared by Sonochemical and Sol-Gel Methods.

25 B. Jaleh and A. Jabbari, Evaluation of reduced graphene oxide/ZnO effect on properties of PVDF nanocomposite films, *Appl. Surf. Sci.*, 2014, **320**, 339–347.

26 A. C. Lopes, C. Caparros, S. Ferdov and S. Lanceros-Mendez, Influence of zeolite structure and chemistry on the electrical response and crystallization phase of poly(vinylidene fluoride), *J. Mater. Sci.*, 2013, **48**, 2199–2206.

27 R. Gregorio Jr, Determination of the α, β, and γ crystalline phases of poly(vinylidene fluoride) films prepared at different conditions, *J. Appl. Polym. Sci.*, 2006, **100**(4), 3272–3279.

28 P. Martins, A. C. Lopes and S. Lanceros-Mendez, Electroactive phases of poly(vinylidene fluoride): determination, processing and applications, *Prog. Polym. Sci.*, 2014, **39**(4), 683–706.

29 R. Gregorio Jr and M. Cestari, Effect of crystallization temperature on the crystalline phase content and morphology of poly(vinylidene fluoride), *J. Polym. Sci., Part B: Polym. Phys.*, 1994, **32**(5), 859–870.

30 S. A. Salman, F. T. Noori and A. K. Mohammed, Preparation and Characterizations of Poly(vinylidene fluoride) (PVDF)/Ba₀.₆Sr₀.₄TiO₃ (BST) Nanocomposites, *Int. J. Appl. Eng. Res.*, 2018, **13**(7), 5008–5013.

31 A. Al-Saygh, D. Ponnamma, M. A. AlMaadeed, P. Vijayan P, A. Karim and M. K. Hassan, Flexible Pressure Sensor Based on PVDF Nanocomposites Containing Reduced Graphene Oxide-Titania Hybrid Nanolayers, *Polymers*, 2017, **9**, 33.

32 J. Dai, K. Xiao, H. Dong, W. Liao, X. Tang, Z. Zhang and S. Cai, Preparation of Al₂O₃/PU/PVDF composite membrane and performance comparison with PVDF membrane, PU/PVDF blending membrane, and Al₂O₃/PVDF hybrid membrane, *Desalin. Water Treat.*, 2016, **57**(2), 487–494.

33 A. M. AlAhzm, M. O. Alejli, D. Ponnamma, *et al.*, Piezoelectric properties of zinc oxide/iron oxide filled polyvinylidene fluoride nanocomposite fibers, *J. Mater. Sci.: Mater. Electron.*, 2021, **32**, 14610–14622.

34 N. Maity, A. Mandal and A. K. Nandi, Hierarchical nanostructured polyaniline functionalized graphene/poly(vinylidene fluoride) composites for improved dielectric performances, *Polymer*, 2016, **103**, 83–97.

35 K. Yang, X. Huang, L. Fang, J. He and P. Jiang, Fluoropolymer functionalized graphene for flexible ferroelectric polymer-based high-k nanocomposites with suppressed dielectric loss and low percolation threshold, *Nanoscale*, 2014, **6**(24), 14740–14753.

36 C. Xing, L. Zhao, J. You, W. Dong, X. Cao and Y. Li, Impact of ionic liquid-modified multiwalled carbon nanotubes on the crystallization behavior of poly(vinylidene fluoride), *J. Phys. Chem. B*, 2012, **116**, 8312–8320.

37 *Broad-band dielectric spectroscopy*, ed. F. Kremer and A. Schönhals, Springer Science & Business Media, 2002.

38 X. Liang, S. Yu, R. Sun, S. Luo, J. Wan, S. Yu, Z. Zhuang, *et al.*). Microstructure and dielectric behavior of the three-phase Ag@SiO$_2$/BaTiO$_3$/PVDF composites with high permittivity, *J. Mater. Res.*, 2012, **27**(7), 991–998.

39 A. P. Indolia and M. S. Gaur, Investigation of structural and thermal characteristics of PVDF/ZnO nanocomposites, *J. Therm. Anal. Calorim.*, 2013, **113**, 821–830.

40 S. Luo, S. Yu, R. Sun and C. P. Wong, Nano Ag-deposited BaTiO$_3$ hybrid particles as fillers for polymeric dielectric composites: toward high dielectric constant and suppressed loss, *ACS Appl. Mater. Interfaces*, 2014, **6**(1), 176–182.

41 A. Sasmal, A. Patra, P. S. Devi and S. Sen, Space charge induced augmented dielectric permittivity and improved energy harvesting ability of nano-Ag decorated ZnSnO$_3$ filled PVDF based flexible nanogenerator, *Compos. Sci. Technol.*, 2021, **213**, 108916.

42 G. Peng, X. Zhao, Z. Zhan, S. Ci, Q. Wang, Y. Liang and M. Zhao, New crystal structure and discharge efficiency of poly(vinylidene fluoride-hexafluoropropylene)/poly(methyl methacrylate) blend films, *RSC Adv.*, 2014, **4**, 16849–16854.

43 S. K. Karan, A. K. Das, R. Bera, S. Paria, A. Maitra, N. K. Shrivastava and B. B. Khatua, Effect of γ-PVDF on enhanced thermal conductivity and dielectric property of Fe-rGO incorporated PVDF based flexible nanocomposite film for efficient thermal manage ment and energy storage applications, *RSC Adv.*, 2016, **6**(44), 37773–37783.

44 K. Shi, B. Sun, X. Huang and P. Jiang, Synergistic effect of graphene nanosheet and BaTiO$_3$ nanoparticles on performance enhancement of electrospun PVDF nanofiber mat for flexible piezoelectric nanogenerators, *Nano Energy*, 2018, **52**, 153–162.

45 D. Mandal, K. Henkel and D. Schmeißer, Improved performance of a polymer nanogenerator based on silver nanoparticles doped electrospun P(VDF–HFP) nanofibers, *Phys. Chem. Chem. Phys.*, 2014, **16**, 10403–10407.

46 H. Parangusan, D. Ponnamma and M. A. A. AlMaadeed, Toward high power generating piezoelectric nanofibers: influence of particle size and surface electrostatic interaction of Ce–Fe$_2$O$_3$ and Ce–Co$_3$O$_4$ on PVDF, *ACS Omega*, 2019, **4**(4), 6312–6323.

47 C. Chen, S. Zhao, C. Pan, et al., A method for quantitatively separating the piezoelectric component from the as-received "piezoelectric" signal, *Nat. Commun.*, 2022, **13**, 1391.